Microelectronics Reliability 50 (2010) 775–789

Contents lists available at ScienceDirect

Microelectronics Reliability

journal homepage: www.elsevier.com/locate/microrel

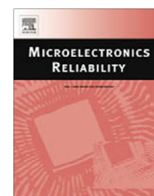

Introductory Invited Paper

Physically based models of electromigration: From Black's equation to modern TCAD models

R.L. de Orio, H. Ceric, S. Selberherr *

Institute for Microelectronics, TU Wien Gußhausstraße 27–29/E360, A-1040 Wien, Austria

ARTICLE INFO

Article history:
Received 14 January 2010
Available online 20 March 2010

Keywords:
Electromigration
Modeling
Interconnects
TCAD

ABSTRACT

Electromigration failure is a major reliability concern for integrated circuits. The continuous shrinking of metal line dimensions together with the interconnect structure arranged in many levels of wiring with thousands of interlevel connections, such as vias, make the metallization structure more susceptible to failure. Mathematical modeling of electromigration has become an important tool for understanding the electromigration failure mechanisms. Therefore, in this work we review several electromigration models which have been proposed over the years. Starting from the early derivation of Black's equation, we present the development of the models in a somewhat chronological order, until the recent developments for fully three-dimensional simulation models. We focus on the most well known, continuum physically based models which have been suitable for comprehensive TCAD analysis.

© 2010 Elsevier Ltd. All rights reserved.

1. Introduction

Electromigration is the process of mass transport caused by the momentum transfer between conducting electrons and metal atoms. As atoms migrate along the line, at sites of flux divergences material accumulation or depletion takes place. Typically, in regions of depletion voids are formed and grow, first causing a significant resistance increase in the line and, finally, leading to line severing.

According to the International Technology Roadmap for Semiconductors (ITRS) 2008 Update [1], the copper dual-damascene technology process will continue to be applied for fabrication of on-chip interconnects for the next technological nodes. The metal wiring pitch in integrated logic circuits will reach as down as 64 nm for the 32 nm node, and 44 nm for the 22 nm node. At the same time, the expected operating current densities can reach 2.11 MA/cm^2 and 2.80 MA/cm^2, respectively [1]. In addition, the interconnect structure is arranged in several levels of wiring with thousands of interlevel connections such as vias. Due to this continuous scaling of on-chip interconnects, where high current densities and temperature operating conditions are unavoidable, electromigration will continue to be a key reliability issue, and the prediction of the long term interconnect behavior is a major necessity.

Since the late 1960s, several models have been proposed to describe electromigration. The main problem is that electromigration is influenced by a wide diversity of physical phenomena and depends on a large number of intrinsic and extrinsic effects. Moreover, the complex interconnect geometries and technological process related features of modern interconnects, such as a typical dual-damascene line of Fig. 1, make modeling even more challenging.

Mathematical modeling can significantly contribute to the understanding of electromigration failure mechanisms. It can be an important tool for explaining several experimental observations and, ultimately, it can provide an improved basis for design and fabrication of reliable metallizations.

In this paper we present various electromigration models which have appeared in the last decades. We start from the very simple, one-dimensional models which consider only the diffusional term and the electromigration itself to describe the vacancy concentration behavior along a simple line. We then proceed to more sound models incorporating the effects of mechanical stress. The complexity gradually increases as we describe more general models, suitable for TCAD analysis of two- and realistic three-dimensional interconnect structures. Here, the effect of fast diffusivity paths and the connection of mechanical stress build-up with material transport and sites of vacancy annihilation or generation, like grain boundaries, are presented. Finally, we discuss the void nucleation condition followed by the description of void evolution models, placing particular emphasis on the available numerical methods which are suitable for TCAD.

2. Black's equation

Based on a very simple model Black [2–4] was first to derive an expression for the time to failure of a metal line subjected to

* Corresponding author.
E-mail address: Selberherr@TUWien.ac.at (S. Selberherr).

0026-2714/$ - see front matter © 2010 Elsevier Ltd. All rights reserved.
doi:10.1016/j.microrel.2010.01.007

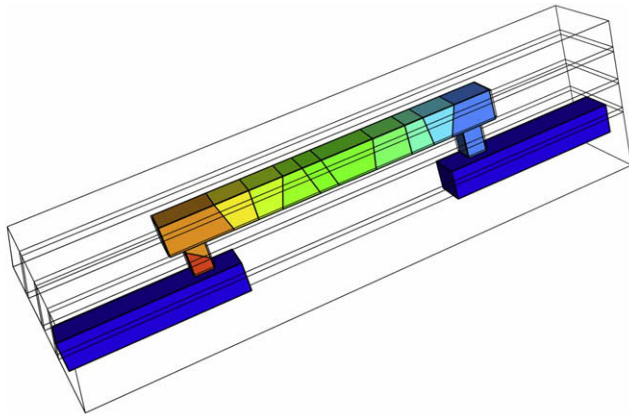

Fig. 1. Typical copper dual-damascene interconnect line.

electromigration. He considered that the mean time to failure, MTF, is inversely proportional to the rate of mass transport, R_m,

$$MTF \propto \frac{1}{R_m}, \tag{1}$$

and that the rate of mass transport is proportional to the momentum transfer between thermally activated ions and conducting electrons,

$$R_m \propto n_e \Delta p N_a, \tag{2}$$

where n_e is the density of conducting electrons, Δp is the momentum transfer from the electrons to the metal atoms, and N_a is the density of thermally activated ions. Furthermore, assuming that both the electron density as well as the momentum transfer are proportional to the current density, j,

$$n_e \propto j, \qquad \Delta p \propto j, \tag{3}$$

and that the activated ions follow an Arrhenius equation

$$N_a \propto \exp(-E_a/kT), \tag{4}$$

the mean time to failure is modeled as

$$MTF = \frac{A}{j^2} \exp\left(\frac{E_a}{kT}\right), \tag{5}$$

where A is a constant which comprises the material properties and the geometry of the interconnect [2,4], E_a is the activation energy, T is the temperature, and k is Boltzmann's constant.

It was observed that not all experimental results followed (5), but they could be fitted by allowing a variable current density exponent. Therefore, Black's equation was modified to [5]

$$MTF = \frac{A}{j^n} \exp\left(\frac{E_a}{kT}\right), \tag{6}$$

where the current density exponent, n, can be experimentally determined.

It is interesting to note that the original Eq. (5) predicted a failure time proportional to the inverse square of the current density, even though mass transport due to electromigration had been shown to be linearly dependent on the current density [6]. This issue was discussed by several authors [5,7], however, the explanation for the square dependence was elucidated only several years later, when various theoretical works [8–13] considerably contributed to a better understanding of the electromigration behavior. An exponent close to 1 indicates that the lifetime is dominated by the void growth mechanisms, i.e. the time for a void to grow and lead to failure represents the major portion of the lifetime [9,10], while a value close to 2 indicates that void nucleation is the dominant phase of the electromigration lifetime [8,11–13].

Eq. (6) has been used for lifetime estimation and extrapolation to operating conditions for 40 years now. However, in a recent publication Lloyd [14] discussed the application of the modified Eq. (6) and concluded that it may lead to significant errors in the lifetime extrapolation. These errors arise from the assumption that the fitting parameters A, E_a, and n obtained from the accelerated tests can be directly applied for the lifetime extrapolation. As Lloyd [14] shows, the experimental measurement of the above parameters does not consider important additional temperature and also pre-existing stress dependences, which yields incorrect parameter values and, consequently, lifetime extrapolation.

Although Black's equation provides useful insight into electromigration failure, it does not allow a thorough understanding of the underlying physics related to the electromigration behavior for which more sophisticated physically based models are required.

3. Electromigration induced material transport equations

Electromigration refers to the transport of material caused by the momentum transfer from conducting electrons to metal atoms [6]. Nevertheless, the total atomic migration is influenced by other physical mechanisms. In general, electromigration constitutes a diffusion–convection problem, where atomic transport along the interconnect line occurs due to a combination of several driving forces. Since the atomic migration occurs via a vacancy exchange mechanism, the material transport can be described in terms of a vacancy flux. The total vacancy flux can be generally written as

$$\vec{J}_v = -D_v\left(\nabla C_v - \frac{|Z^*|e}{kT} C_v \vec{E} - \frac{Q^*}{kT^2} C_v \nabla T + \frac{f\Omega}{kT} C_v \nabla \sigma\right), \tag{7}$$

where D_v is the vacancy diffusivity, C_v is the vacancy concentration, Z^* is the effective charge number, e is the elementary charge, $\vec{E}$ is the electric field, Q^* is the heat of transport, f is the vacancy relaxation factor, Ω is the atomic volume, σ is the hydrostatic stress, k is Boltzmann's constant, and T is the temperature. This equation contains all driving forces for material transport, namely, the diffusional term given by the gradient of the vacancy concentration, the electromigration itself, and the driving forces due to gradients of temperature and gradients of mechanical stress.

In sites of flux divergence vacancies can accumulate or vanish, and the material balance is given by

$$\frac{\partial C_v}{\partial t} = -\nabla \cdot \vec{J}_v + G, \tag{8}$$

where G represents a generation or annihilation term.

Eqs. (7) and (8) are the basic continuum equations which describe the total mass transport that occurs along an interconnect line. Below we present several works which have appeared in order to model the electromigration behavior. We start the description from the very simple, one-dimensional models which consider only the diffusional term and the electromigration itself to describe the vacancy concentration behavior along a simple line, and we gradually advance towards the more complete TCAD models which take into account the effect of fast diffusivity paths, connect the mechanical stress build-up to sites of vacancy annihilation or generation, and are able to handle complex three-dimensional interconnect structures. Then, we discuss the void nucleation condition followed by the description of void evolution models and available numerical approaches.

3.1. One-dimensional diffusive models

The model proposed by Shatzkes and Lloyd [8] was the first that rigorously derived the interconnect lifetime with an inverse square

dependence on current density. Considering the influence of diffusion and electromigration only on the vacancy flux, the continuity Eq. (8) along the interconnect length direction can be written as

$$\frac{\partial C_v}{\partial t} = D_v \frac{\partial^2 C_v}{\partial x^2} - \frac{D_v |Z^*| e\rho j}{kT} \frac{\partial C_v}{\partial x}, \tag{9}$$

where the source term $G = 0$ is used.

For a semi-infinite line under the boundary conditions

$$C_v(-\infty, t) = C_{v0} \quad \text{and} \quad J_v(0, t) = 0, \tag{10}$$

which means that the vacancy concentration at $x = -\infty$ is fixed at an initial equilibrium value, C_{v0}, and that there is a perfect blocking boundary ($J_v = 0$) at $x = 0$, the solution of (9) at the blocking boundary is given by Laplace transformations [8]

$$\frac{C_v(0,t)}{C_{v0}} = 1 + \mathrm{erf}\beta + 2\left[\beta^2(1 + \mathrm{erf}\beta) + \frac{\beta}{\sqrt{\pi}} \exp(-\beta^2)\right], \tag{11}$$

where

$$\beta = \frac{|Z^*| e\rho j}{2kT} \sqrt{D_v t}. \tag{12}$$

Assuming that the failure occurs, when the vacancy concentration reaches a given critical value C_{vf} significantly higher than the initial equilibrium value C_{v0}, and that $\beta \gg 0$, then (11) is approximated [8] by

$$C_{vf}/C_{v0} \approx 4\beta^2 = \left(\frac{|Z^*| e\rho j}{kT}\right)^2 D_v t_f. \tag{13}$$

Since the diffusion coefficient is expressed by the Arrhenius relation

$$D_v = D_{v0} \exp\left(-\frac{E_a}{kT}\right), \tag{14}$$

where D_{v0} is the pre-exponential factor for vacancy diffusivity, (13) yields the mean time to failure of the form

$$MTF = \frac{AT^2}{j^2} \exp\left(\frac{E_a}{kT}\right). \tag{15}$$

Note that the above equation is similar to the original Black's Eq. (5), except for the multiplying term T^2, and it also predicts a mean time to failure with an inverse square current density dependence. This is a result of the assumption that the failure takes place, when the vacancy concentration reaches a given critical value, which corresponds, in fact, to a void nucleation condition.

A more interesting solution of (9) is obtained for a finite line with blocking boundary conditions at both ends of the line, i.e.

$$J_v(0, t) = J_v(-L, t) = 0, \tag{16}$$

where l is the line length, so that the solution becomes [15]

$$\frac{C_v(x,t)}{C_{v0}} = A_0 - \sum_{n=1}^{\infty} A_n \exp\left(-B_n \frac{D_v}{L^2} t + \frac{\alpha}{2} \frac{x}{L}\right), \tag{17}$$

where

$$\alpha = \frac{|Z^*| e\rho j L}{kT}, \tag{18}$$

the steady-state solution is determined by the term

$$A_0 = \frac{\alpha}{1 - \exp(-\alpha)} \exp\left(\alpha \frac{x}{L}\right), \tag{19}$$

and

$$A_n = \frac{16 n\pi\alpha^2 [1 - (-1)^n \exp(\alpha/2)]}{(\alpha^2 + 4n^2\pi^2)^2} \left[\sin\left(n\pi \frac{x}{L}\right) + \frac{2n\pi}{\alpha} \cos\left(n\pi \frac{x}{L}\right)\right], \tag{20}$$

$$B_n = n^2\pi^2 + \alpha^2/4. \tag{21}$$

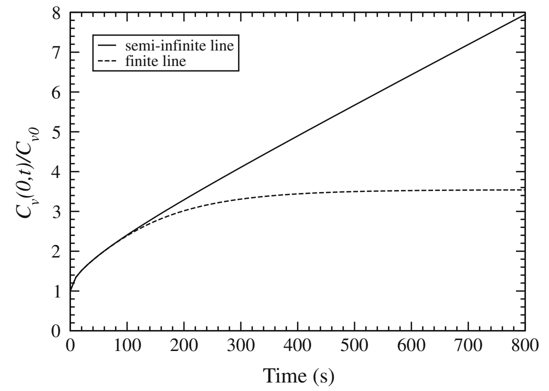

Fig. 2. Vacancy concentration at the blocking boundary at $x = 0$ for the semi-infinite line, (11), and the finite-line, (17).

Table 1
Parameters used in the calculations.

Parameter	Value	Reference
D_{v0}	0.052 cm^2/s	[16]
E_a	0.9 eV	[17]
Z^*	−5.0	[18]
ρ	1.69×10^{-6} Ω cm	[16]
j	2 MA/cm^2	–
L	100 μm	–
T	573 K	–

Fig. 2 shows the vacancy concentration evolution with time at the blocking boundary at $x = 0$ for a semi-infinite and a 100 μm long line with $\alpha \approx 3.4$. The semi-infinite line and the finite line solution agree well for early times and significantly deviate at longer times. Using the parameters given in Table 1 the vacancy concentration in the finite line already saturates after about 10 min. This is a very short time compared to the failure times obtained from experiments, which are in the order of several hours.

Fig. 3 shows the vacancy concentration along the finite line at different times. As vacancies drift from the anode end to the cathode end of the line a gradient in vacancy concentration develops, which counters the electromigration flux. As a result, the net vacancy flux is reduced, until it vanishes, and the steady-state condition given by (19) is reached.

Such a short time to reach the steady-state was previously observed by Rosenberg and Ohring [19]. Their electromigration model is similar to that given by (9), but it includes a source term so that

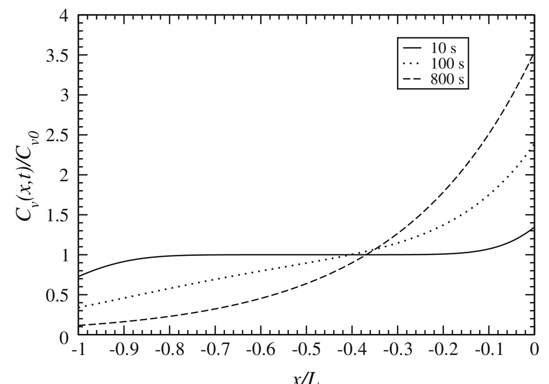

Fig. 3. Vacancy concentration along the line at different times according to (17).

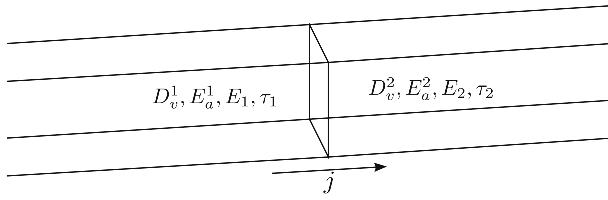

Fig. 4. Grains with different properties forming a grain boundary.

$$\frac{\partial C_v}{\partial t} = D_v \frac{\partial^2 C_v}{\partial x^2} - D_v \frac{|Z^*|eE}{kT}\frac{\partial C_v}{\partial x} - \frac{C_v - C_{v0}}{\tau}, \tag{22}$$

where C_{v0} is the equilibrium vacancy concentration and τ is the characteristic vacancy relaxation time. The last term of the right-hand side of this equation represents a source function which models vacancy annihilation and generation. It means that vacancies are annihilated, if their concentration is larger than the equilibrium value, or produced, if their concentration is smaller than the equilibrium one. The vacancy relaxation time, τ, characterizes the efficiency of the sites acting as sink/sources, in such a way that smaller values of τ result in shorter times for the vacancy concentration to reach the steady-state condition, and vice versa.

It was observed that the damage site locations were related to specific grain boundary configurations, in such a way that most of the failures occurred at sites of significant change in the grain size [20]. Considering the intersection of two grains forming a grain boundary, as shown in Fig. 4, Rosenberg and Ohring analyzed the vacancy supersaturation that can be achieved at the grain boundary, when the grains have different properties [19]. It means that differences in the diffusivities or in the number of diffusion pathways on each grain can lead to a higher flux divergence at the grain boundary. At steady-state ($\partial C_v/\partial t = 0$) both, the vacancy concentration and the flux, are continuous along the grain boundary interface

$$C_v^1(x=0) = C_v^2(x=0) \quad \text{and} \quad J_v^1(x=0) = J_v^2(x=0), \tag{23}$$

so that the solution of (22) yields for each grain [19]

$$\begin{aligned} S_1(x) &= \frac{C_v^1(x) - C_{v0}}{C_{v0}} = S(0)\exp(-\lambda_1 x), \quad x < 0 \\ S_2(x) &= \frac{C_v^2(x) - C_{v0}}{C_{v0}} = S(0)\exp(-\lambda_2 x), \quad x > 0 \end{aligned} \tag{24}$$

where $S(0)$ is the vacancy supersaturation at $x = 0$, given by

$$S(0) = \left[\left(\frac{\lambda_1 D_v^1 - \lambda_2 D_v^2}{D_v^2 E_2 - D_v^1 E_1}\right)\frac{kT}{|Z^*|e} - 1\right]^{-1}, \tag{25}$$

and

$$\begin{aligned} \lambda_1 &= -\frac{|Z^*|eE_1}{2kT} - \left[\left(\frac{|Z^*|eE_1}{2kT}\right)^2 + \frac{1}{D_v^1\tau_1}\right]^{1/2} \\ \lambda_2 &= -\frac{|Z^*|eE_2}{2kT} + \left[\left(\frac{|Z^*|eE_2}{2kT}\right)^2 + \frac{1}{D_v^2\tau_2}\right]^{1/2} \end{aligned} \tag{26}$$

Using the parameters given in Table 1 and assuming the activation energies $E_a^1 = 0.8$ eV and $E_a^2 = 1.0$ eV for the left and right grain, respectively, the vacancy supersaturation along the grains for different vacancy relaxation times is shown in Fig. 5. We can see that the supersaturation significantly decreases as the vacancy relaxation time decreases. Furthermore, the maximum supersaturation is rather small, even for longer vacancy relaxation times. This means that the maximum supersaturation is significantly dependent on τ, that is, it is significantly dependent on the effectiveness of the vacancy sink/source. As a consequence, high vacancy supersaturation cannot be obtained near vacancy sinks, since vacancies are annihilated as soon as the local vacancy concentration becomes higher than its equilibrium value.

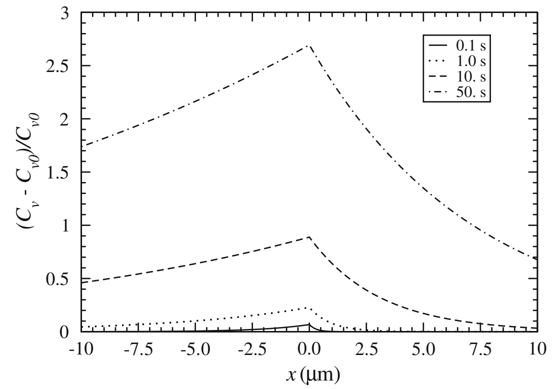

Fig. 5. Steady-state vacancy supersaturation for different values of the characteristic vacancy relaxation time τ.

Based on the classical homogeneous nucleation theory Rosenberg and Ohring [19] showed that the energy barrier for void formation would be extremely high for the calculated vacancy supersaturations. Therefore, the authors recognized that void nucleation by vacancy condensation could not occur, unless heterogeneous nucleation sites were present.

The time development of the vacancy supersaturation at the grain boundary is presented in Fig. 6. The time to reach the steady-state condition is in the order of seconds, which is too short compared to the typical failure times. Even for much larger vacancy relaxation times the time to reach the steady-state is in the order of minutes, at most.

These observations led Rosenberg and Ohring to conclude that void formation due to electromigration was likely to be fast, so that the electromigration lifetime was supposed to be dominated by void growth mechanisms, like void growth at a grain boundary triple point or by grain boundary grooving [19,21].

The aforementioned models, where material transport only due to gradients of concentration and due to electromigration itself is considered, have two main shortcomings: the time scale to reach the steady state vacancy supersaturation is too short and the maximum vacancy supersaturation is very low, which hinders void formation by means of vacancy condensation. Therefore, a critical vacancy concentration cannot be used to determine the failure of the interconnect. As will be shown in the next sections, these

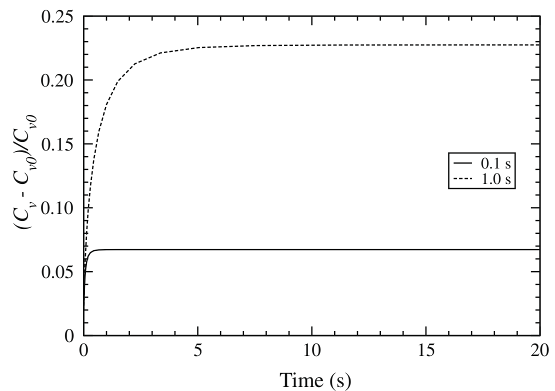

Fig. 6. Vacancy supersaturation at the grain boundary as a function of time for $\tau = 0.1$ s and 1.0 s obtained from numerical simulations.

shortcomings can only be resolved with the introduction of mechanical stress in the model equations.

4. Electromigration and mechanical stress

In the previous section was shown that the drift of vacancies towards the cathode end of an interconnect line due to electromigration leads to accumulation of vacancies in this region and, at the same time, leads to vacancy depletion at the anode end. Since there is a small relaxation of the lattice surrounding a vacancy, vacancy accumulation would produce volume contraction at the cathode. In turn, the depletion of vacancies would produce volume expansion at the anode end. However, due to the constraints imposed by the surrounding layers, namely, the capping layer, the barrier layer, and the passivation in copper dual-damascene interconnects, these volumetric changes cannot be accommodated, which results in the development of mechanical stress in the line. At the cathode end tensile stress is produced, while compressive stress develops at the anode end of the line. As will be shown below, this stress gradient acts as an additional driving force for material transport and must be taken into account in the vacancy flux equation. Moreover, mechanical stress is a key parameter for the void nucleation condition.

4.1. The Blech effect

Blech [22–24] designed an experiment where conductor islands were deposited onto a titanium nitride (TiN) film and stressed at a high current density. As the conductor resistivity was much lower than that of the TiN layer, the conductor stripe would carry most of the current and the resulting movement of the ends of the stripe could be measured. In this way, the electromigration induced drift velocity is determined by

$$v_d = \frac{D_a|Z^*|e\rho j}{kT}, \tag{27}$$

where D_a is the atomic diffusivity.

Blech observed that only the upstream end (in relation to the electron flow) of the line moved according to (27), and that the upstream end stopped moving, when the stripe reduced to a certain length. Also, he observed that no drift could be detected below a threshold current density.

These observations can be explained by considering the flux due to electromigration and the gradient of chemical potential via a gradient of mechanical stress [22–25] according to

$$J_v = \frac{D_v C_v}{kT}\left(|Z^*|e\rho j - \Omega\frac{\partial\sigma}{\partial x}\right), \tag{28}$$

where Ω is the atomic volume and σ is the hydrostatic stress. This equation shows that a gradient of mechanical stress acts as driving force against electromigration. Thus, electromigration stops, when the opposing stress gradient, commonly referred to as "back stress", equals the electromigration driving force, so that $J_v = 0$. This steady-state condition is the so-called "Blech Condition", given by

$$\frac{\partial\sigma}{\partial x} = \frac{|Z^*|e\rho j}{\Omega}. \tag{29}$$

Integrating (29) over the length of the interconnect line yields

$$\sigma(x) = \sigma_0 + \frac{|Z^*|e\rho j}{\Omega}x, \tag{30}$$

where σ_0 is the stress at $x = 0$. This equation shows that the stress varies linearly along the line, when the backflow flux equals the electromigration flux.

Given that the maximum stress the conductor line can withstand is σ_{th}, a critical product for electromigration failure can be stated as

$$(jL)_c = \frac{\Omega(\sigma_{th} - \sigma_0)}{|Z^*|e\rho}. \tag{31}$$

This is the so-called "Blech Product". The critical product provides a measure of the interconnect resistance against electromigration failure and several experimental works have reported that the critical product for modern copper interconnects is in the range from 2000 to 10,000 A/cm [26–29].

From the above expression, for a given current density, j, we can determine a critical line length, so that shorter lines will not fail due to electromigration. This is known as "Blech Length", given by

$$l_B = \frac{\Omega(\sigma_{th} - \sigma_0)}{|Z^*|e\rho j}. \tag{32}$$

Similarly, for a given line length, L, the maximum current density that can be applied for which electromigration failure does not occur is

$$j_c = \frac{\Omega(\sigma_{th} - \sigma_0)}{|Z^*|e\rho L}. \tag{33}$$

An important consequence of the Blech effect is that the jL product during electromigration tests has to be significantly higher than the critical product $(jL)_c$ for the corresponding test structure. Otherwise, the test structure might fail at longer times than it would normally do, giving a false sense of safety [30]. Another point to be mentioned is that the presence of residual stresses from the fabrication process reduces the stress which has to be produced by electromigration in order to reach the maximum value the line can withstand. This results in smaller values for the Blech length and for the maximum operating current density than that given by (32) and (33), respectively [30].

4.2. Electromigration induced stress

Although Blech had shown that electromigration transport was closely related to mechanical stress development, the first model that connected the rate of stress generation to electromigration was proposed by Kirchheim [11]. He added the gradient of mechanical stress as a driving force in the total vacancy flux equation, so that

$$J_v = -D_v\left(\frac{\partial C_v}{\partial x} - \frac{|Z^*|e\rho j}{kT}C_v + \frac{f\Omega}{kT}C_v\frac{\partial\sigma}{\partial x}\right), \tag{34}$$

where $f = \Omega_v/\Omega$. Thus, the continuity equation can be written as

$$\frac{\partial C_v}{\partial t} = -\frac{\partial}{\partial x}\left[-D_v\left(\frac{\partial C_v}{\partial x} - \frac{|Z^*|e\rho j}{kT}C_v + \frac{f\Omega}{kT}C_v\frac{\partial\sigma}{\partial x}\right)\right] - \frac{C_v - C_{veq}}{\tau}. \tag{35}$$

The last term is a generation/annihilation function similar to that proposed by Rosenberg and Ohring [19], as shown in Section 3.1. However, Kirchheim used the more general expression for the equilibrium vacancy concentration in a grain boundary [31]

$$C_{veq} = C_{v0}\exp\left[\frac{(1-f)\Omega\sigma}{kT}\right], \tag{36}$$

which connects the equilibrium vacancy concentration with mechanical stress.

The volumetric strain in a grain produced by the generation of vacancies is [11]

$$\frac{\Delta V}{V} = (1-f)\Omega\frac{\delta}{d}\Delta C_v, \tag{37}$$

where $(1-f)\Omega$ is the volume change due to lattice relaxation, when a vacancy is treated as a substitutional atom with smaller volume $(0 < f < 1)$, δ is the grain boundary thickness, d is the grain diameter, and ΔC_v is the generated vacancy concentration. Thus, the strain rate is given by

$$\frac{1}{V}\frac{\partial V}{\partial t} = (1-f)\Omega\frac{\delta}{d}\frac{C_v - C_{veq}}{\tau}, \tag{38}$$

which together with Hooke's law yields

$$\frac{\partial \sigma}{\partial t} = B(1-f)\Omega\frac{\delta}{d}\frac{C_v - C_{veq}}{\tau}, \tag{39}$$

where B is the appropriate modulus.

This equation shows that the stress build-up is related to the deviation of the vacancy concentration from its equilibrium value and that τ can have a significant impact on the stress development. It is important to note that this model allows different mechanisms of vacancy annihilation or generation to be described, such as annihilation/production in the grain boundary itself, in adjacent grain boundaries or at dislocations within the grain bulk. These lead to smaller, median, and larger values of the characteristic vacancy relaxation time τ, respectively.

Eqs. (35) and (39) compose a non-linear system of differential equations which has to be solved numerically. Nevertheless, Kirchheim derived analytical solutions for some limiting cases and identified three main phases for vacancy and stress evolution [11]. The first phase corresponds to a short period of time, where the initial stress is very low. Therefore, the equilibrium vacancy concentration remains unaffected and the vacancy concentration develops until a quasi steady-state condition is reached. The quasi steady-state phase is quite long, and the vacancy concentration does not change very much, while the stress grows linearly with time. It lasts until the stress becomes large enough to affect the equilibrium vacancy concentration. Then, a non-linear increase of stress with time is observed and the vacancy concentration approximately follows the development of the equilibrium vacancy concentration, which means that vacancies and stresses are in equilibrium and the true steady-state condition has been reached.

Moreover, Kirchheim [11] showed that, if the electromigration lifetime is determined by the time to reach a certain critical stress, the current density exponent of Black's equation varies from $n = 1$ at low stresses (the time to failure is determined by the quasi steady-state period) to $n = 2$ for higher critical stresses (the time to reach the true steady-state condition determines the lifetime).

A somewhat simplified model for the stress development in a line subject to electromigration was derived by Korhonen et al. [12]. They consider that the generation/recombination of vacancies by dislocation climb mechanisms either in grain boundaries or at lattice dislocations changes the concentration of lattice sites, C_L, producing stress according to Hooke's law

$$\frac{dC_L}{C_L} = -\frac{d\sigma}{B}. \tag{40}$$

Using the source term [13,32]

$$G = \frac{\partial C_L}{\partial t}, \tag{41}$$

the vacancy continuity equation can be written as

$$\frac{\partial C_v}{\partial t} = -\frac{\partial J_v}{\partial x} - \frac{C_L}{B}\frac{\partial \sigma}{\partial t}. \tag{42}$$

Assuming that the vacancy concentration is in equilibrium with the mechanical stress via [31]

$$C_v = C_{veq} = C_{v0}\exp\left(\frac{\Omega\sigma}{kT}\right), \tag{43}$$

(42) becomes

$$\left(\frac{C_v B\Omega}{C_L kT} + 1\right)\frac{C_L}{B}\frac{\partial \sigma}{\partial t} = \frac{\partial}{\partial x}\left[\frac{D_v C_v}{kT}\left(\Omega\frac{\partial \sigma}{\partial x} - |Z^*|e\rho j\right)\right], \tag{44}$$

with J_v given by (28).

Korhonen et al. observed that $(C_v/C_L)(B\Omega/kT) \ll 1$ at typical electromigration test conditions. This means that most of the transported vacancies initiate climbing dislocation processes that produce mechanical stress, while just a very small number of vacancies is needed to maintain the local equilibrium concentration [12]. Thus, the above approximation leads to

$$\frac{\partial \sigma}{\partial t} = \frac{\partial}{\partial x}\left[\frac{D_a B\Omega}{kT}\left(\frac{\partial \sigma}{\partial x} - \frac{|Z^*|e\rho j}{\Omega}\right)\right], \tag{45}$$

where $D_a = D_v C_v / C_L$ [33].

For a line of length L with blocking boundary conditions

$$J_v(0,t) = J_v(-L,t) = 0, \tag{46}$$

and for a constant D_a, the solution of (45) is given by [12,34]

$$\sigma(x,t) = \frac{|Z^*|e\rho jL}{\Omega}\left[\frac{1}{2} + \frac{x}{L} - 4\sum_{n=0}^{\infty} m_n^{-2}\exp\left(-m_n^2\frac{\kappa}{L^2}t\right)\times\cos\left(m_n\frac{x}{L}\right)\right], \tag{47}$$

where we have substituted

$$\kappa = \frac{D_a B\Omega}{kT}, \tag{48}$$

and used the notation $m_n = (2n+1)\pi$.

Following the same approach as Korhonen et al., Clement et al. [13,32] derived an equivalent equation in terms of vacancies,

$$\frac{\partial C_v}{\partial t} = \frac{D_a B\Omega}{kT}\left(\frac{\partial^2 C_v}{\partial x^2} - \frac{|Z^*|e\rho j}{kT}\frac{\partial C_v}{\partial x}\right). \tag{49}$$

This equation has the same form as (9) from the Shatzkes and Lloyd formulation, but with D_v replaced by $D_a B\Omega/kT$. Therefore, the solution for a finite line with blocking boundary conditions at both ends is the same as given by (17)–(21), but with the aforementioned replacement. Since it was assumed that vacancies are in equilibrium with stress, the stress can be calculated from (43) as

$$\sigma(x,t) = \frac{kT}{\Omega}\ln\left[\frac{C_v(x,t)}{C_{v0}}\right], \tag{50}$$

where $C_v(x,t)$ is determined by the solution of (49).

Assuming that the electromigration failure is determined by the time to reach a given stress magnitude, the above models predict a mean time to failure of the form

$$MTF = \frac{B(T)}{j^2}\exp\left(\frac{E_a}{kT}\right). \tag{51}$$

where an inverse square dependence of the current density is again obtained. The coefficient $B(T)$ is temperature dependent, so that $B(T) \propto T^2$ for Korhonen's formulation [12] and $B(T) \propto T^3$ according to Clement's formulation [32].

Fig. 7 shows the stress development with time at $x = 0$ according to Korhonen's solution, (47), using the parameters from Table 1 together with $D_a = 10^{-6}D_v, B = 50$ GPa, and $\Omega = 1.18 \times 10^{-29}$ m^3 [12]. Note that the time scale of stress build-up is in the order of several hours, rather than a few minutes as predicted by the models of Section 3.1. This shows the importance of taking into account the mechanical stress in the model, including the stress dependence in the sink/source term of the continuity equation. The stress distribution along the line for several times is presented in Fig. 8. At steady-state the stress varies linearly, as predicted by Blech [22–24]. We can see that high stress can develop in the intercon-

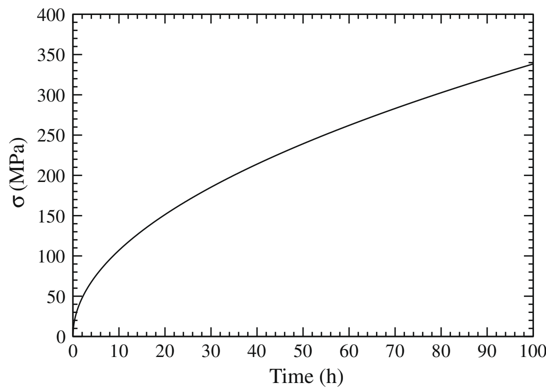

Fig. 7. Stress build-up at $x = 0$ according to Korhonen's model.

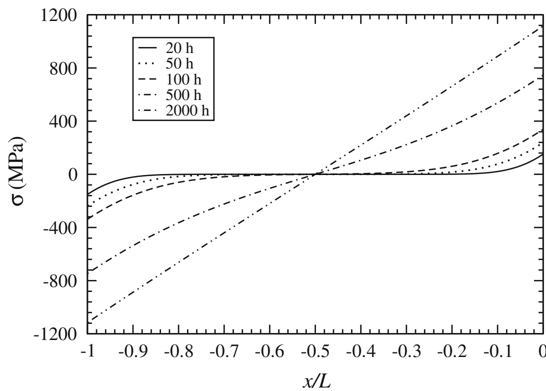

Fig. 8. Stress build-up along the interconnect at different times.

nect line, which is a critical requirement for void nucleation [35,36].

5. TCAD approach for electromigration simulation

The models presented in the previous section greatly contributed to the understanding of the electromigration behavior. Their main advantage is that analytical solutions can be derived for stress evolution during electromigration. However, these solutions are based on several simplifications and apply for idealized cases only. The impact of the complex structure of modern interconnects and general constraints imposed by the surrounding layers on the stress evolution cannot be obtained. Therefore, the development of TCAD approaches has become more and more important, as they have allowed numerical simulations of complete two- [16,37–42] and three-dimensional [43–45] interconnect structures taking into account various physical effects related to electromigration in a consistent manner.

In general, electromigration modeling and simulation constitutes a multi-physics problem which can be subdivided in smaller parts. Typically, electromigration induced failures show two distinctive phases [46]. In the first one no electromigration generated voids can be observed in the interconnect and no significant resistance change of the line occurs. This phase lasts until a void is nucleated. Then, the second phase starts, where the void can evolve in several different ways, until it finally grows to a critical size causing a significant resistance increase or completely severing the interconnect line. As different physical phenomena are responsible for each phase of failure development, electromigration modeling is normally subdivided into the void nucleation

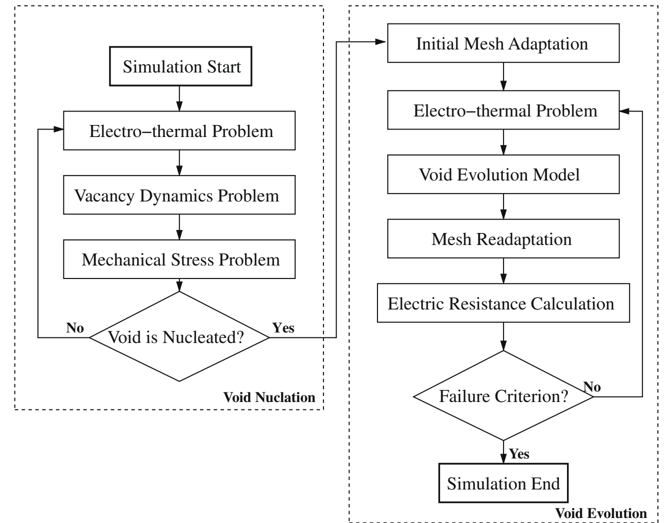

Fig. 9. Schematic procedure for electromigration simulation composed of a void nucleation and a void evolution phase.

phase and the void evolution phase. This is depicted in the typical simulation scheme of Fig. 9. In this way the total electromigration lifetime is the sum of the time for a void to nucleate plus the time for the void to develop, until it leads to the interconnect failure.

The electro-thermal analysis has to be performed in order to obtain the electric potential and temperature distribution in the interconnect. Then, the material balance equation taking into account the various driving forces for mass transport has to be solved, followed by the solution of the mechanical problem. This procedure is repeated until the critical stress for void nucleation is reached. Once a void is formed an initial mesh adaptation may be performed. Since the void changes the local electric field and current density, the electro-thermal analysis has to be again carried out, before the void evolution is actually tracked. Depending on the numerical approach a remeshing routine might be executed. This procedure is repeated continuously, until the interconnect resistance increases to a given threshold value which determines the interconnect failure. This variety of physical effects turns numerical simulations of electromigration into a complex problem which can be further complicated by the consideration of the different material layers existent in a complete interconnect structure and also by the introduction of the microstructure.

As mentioned before, the connection between material transport with mechanical stress in a general framework is a key issue for electromigration simulation. Stresses result from deformations of the metal line volume. Povirk [47] and Rzepka et al. [48] considered that mass accumulation or depletion in the metal line leads to an inelastic strain rate of the form

$$\frac{\partial \varepsilon_{ij}^{i}}{\partial t} = \Omega(\nabla \cdot \vec{J}_v)\delta_{ij}, \tag{52}$$

where δ_{ij} is Kronecker's symbol.

Sarychev et al. [49] proposed an even more general formulation, where the total inelastic strain rate has a contribution from vacancy accumulation/depletion,

$$\frac{\partial \varepsilon_{ij}^{m}}{\partial t} = \frac{1}{3} f\Omega\left(\nabla \cdot \vec{J}_v\right)\delta_{ij}, \tag{53}$$

and a contribution from vacancy generation/annihilation,

$$\frac{\partial \varepsilon_{ij}^{g}}{\partial t} = \frac{1}{3}(1 - f)\Omega G\delta_{ij}, \tag{54}$$

yielding the total inelastic strain rate

$$\frac{\partial \varepsilon_{ij}^{i}}{\partial t} = \frac{1}{3}\Omega[f\nabla\cdot\vec{J}_v + (1-f)G]\delta_{ij}. \quad (55)$$

Assuming that the metal line deforms elastically, so that

$$\sigma_{ij} = \sum_{kl} C_{ijkl}\varepsilon_{kl}, \quad (56)$$

where C_{ijkl} is the stiffness matrix, and using the small displacement approximation,

$$\varepsilon_{ij} = \frac{1}{2}\left(\frac{\partial u_i}{\partial x_j} + \frac{\partial u_j}{\partial x_i}\right), \qquad i,j = 1,2,3 \quad (57)$$

from the mechanical equilibrium equation,

$$\sum_{j=1}^{3}\frac{\partial \sigma_{ij}}{\partial x_j} = 0, \qquad i = 1,2,3 \quad (58)$$

the deformation of the line as a function of the inelastic strain produced by electromigration can be calculated by [49]

$$\mu\nabla^2 u_i + (\lambda+\mu)\frac{\partial}{\partial x_i}(\nabla\cdot\vec{u}) = B\frac{\partial}{\partial x_i}\mathrm{tr}(\varepsilon_{ij}^{i}), \quad i = 1,2,3 \quad (59)$$

where $\vec{u} = (u_1, u_2, u_3)$ is the displacement vector, λ and μ are the Lamé constants, B is the bulk modulus, and $\mathrm{tr}\left(\varepsilon_{ij}^{i}\right)$ refers to the trace of the inelastic strain.

The key characteristic of the above approach is that it forms a three-dimensional self-consistent model which connects material balance with line deformation. In this way, the impact of the complete interconnect geometry and imposed boundary conditions on the stress evolution can be described. Furthermore, all components of the stress tensor can be determined.

Sarychev's model was the basis of several works on simulation of stress evolution due to electromigration [37–39,50] in two-dimensional lines. However, it does not take into account fast diffusivity paths and specific vacancy annihilation/generation rates at the different sites where these processes occur. This was accomplished by Sukharev et al. [16,40–42].

Sukharev et al. [16] wrote the continuity equation, (8), separately for bulk and interfaces,

$$\begin{aligned}\frac{\partial C_v^{bulk}}{\partial t} &= -\nabla\cdot\vec{J}_v^{bulk} \\ \frac{\partial C_v^{int}}{\partial t} &= -\nabla\cdot\vec{J}_v^{int} + G_{int}\end{aligned} \quad (60)$$

where the interfaces, in general, refer to grain boundaries, the Cu/capping layer interface, and the Cu/barrier layer interface. The fluxes along bulk and interfaces are the same as given in (7), but with D_v replaced by the corresponding diffusion coefficient. In this way the vacancy flux along each path is characterized by its own diffusivity. Another important point is that each interface which acts as vacancy sink/source can be described by a specific vacancy annihilation/generation rate.

Sukharev et al. [16] also introduced the concept of plated atoms to describe the atom exchange between bulk and interfaces. He suggested that the event of vacancy generation or annihilation is simultaneously accompanied by atom plating or removal from the grain boundary region, respectively. Therefore, the rate of atom plating/removal is given by the same source function as for vacancies,

$$G_{int} = -\frac{C_v^{int} - C_{veq}}{\tau}. \quad (61)$$

However, considering the plated atoms to be immobile (the atomic mobility is far smaller than the vacancy mobility), the plated atom continuity equation for bulk and interfaces, respectively, are given by [16]

$$\begin{aligned}\frac{\partial C_a^{bulk}}{\partial t} &= 0 \\ \frac{\partial C_a^{int}}{\partial t} + G_{int} &= 0\end{aligned} \quad (62)$$

where C_a refers here to the plated atom concentration.

Based on this concept, Sukharev et al. [16] suggested for the electromigration induced strain

$$\varepsilon_{ij}^{i} = \Omega[-(1-f)(C_v - C_{v0}) + (C_a - C_{a0})]\delta_{ij}, \quad (63)$$

where C_{a0} is the plated atom concentration at the zero-stress condition. This equation shows a close connection between the local strain with the vacancy concentration and the plated atom concentration. However, Sukharev et al. [16] observed that the increment of the plated atom concentration is the major responsible cause for stress build-up.

A somewhat different approach for modeling the grain boundary as a vacancy source/sink was proposed by Ceric et al. [45]. The grain boundary, as depicted in Fig. 10, is treated as a separate region which can trap or release vacancies according to the flux divergence, so that the generation/recombination of vacancies is described by

$$G = \frac{J_{v,1} - J_{v,2}}{\delta_{gb}}. \quad (64)$$

The incoming and outgoing fluxes that result in generation/annihilation processes are given by [45,51]

$$\begin{aligned}J_{v,1} &= \omega_T\left(C_{veq} - C_v^{im}\right)C_v^1 - \omega_R C_v^{im} \\ J_{v,2} &= -\omega_T\left(C_{veq} - C_v^{im}\right)C_v^2 + \omega_R C_v^{im}\end{aligned} \quad (65)$$

where ω_T is the trapping rate of vacancies from both neighboring grains, ω_R is the release rate, C_v^{im} is the trapped vacancy concentration, and C_{veq} is the equilibrium vacancy concentration in the grain boundary. The combination of (64) with (65) yields

$$G = -\frac{\partial C_v^{im}}{\partial t} = \frac{1}{\tau_{gb}}\left\{C_{veq} - C_v^{im}\left[1 + \frac{2\omega_R}{\omega_T(C_v^1 + C_v^2)}\right]\right\}, \quad (66)$$

where

$$\frac{1}{\tau_{gb}} = \frac{\omega_T(C_v^1 + C_v^2)}{\delta_{gb}}. \quad (67)$$

This model has allowed the simulation of a whole interconnect line structure to be carried out in a rather complete way by also taking into account the effects of material interfaces and grain boundaries.

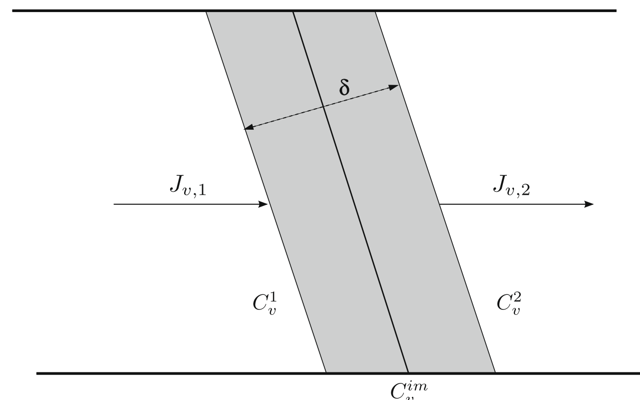

Fig. 10. Schematic grain boundary from Ceric et al. [45].

It has been shown that high stress can develop at grain boundaries away from the cathode end of the line [45], where voids have frequently seen to nucleate [46,52–55]. Sukharev et al. showed that the failure mechanism dramatically changes according to the dominant diffusivity path [16,41,42,56,57]. When the copper/capping layer interface is the dominant diffusivity path, the failure typically occurs by a void that forms at this interface, migrates to the cathode end of the line, and grows [55]. However, if the copper/capping layer goes through a strengthening process [57,58], in such a way that the diffusivity along this path is reduced to the same level as that of grain boundaries, grain boundary diffusion and diffusion along the copper/barrier layer interface play a more important role. As a consequence, void nucleation and growth at the bottom of the via becomes the dominant failure mode [41,42,56–58].

6. Void nucleation condition

Initially, void nucleation was attributed to the accumulation of vacancies at sites of flux divergence caused by their drift due to electromigration. As the vacancy concentration at a particular site reached a certain critical magnitude, vacancy condensation would lead to the formation of a void [8–10,40,43,44,59,60]. However, an unrealistically high vacancy supersaturation would be necessary for spontaneous void formation by vacancy condensation [19,61]. Therefore, according to classical thermodynamics homogeneous void nucleation by a vacancy condensation mechanism cannot be supported under electromigration.

Meanwhile, several works investigated the impact of mechanical stress on void nucleation at various conditions [62–65]. The importance of mechanical stress build-up in an interconnect line under electromigration was recognized, so that the development of a critical stress became the major criterion for void formation [11,12,32,39,45]. Nevertheless, the stress threshold value was still an open issue, varying from work to work.

Gleixner et al. [36] carried out a thorough analysis of the nucleation rates at various locations within an interconnect line, namely, homogeneous nucleation by vacancy condensation, nucleation at a grain boundary, at the line sidewall in the presence and absence of an intersecting grain boundary, and at an interface notch. For all cases the nucleation rates are far too low. Therefore, none of these mechanisms can lead to void formation.

Flinn [35] proposed that a void could form at a pre-existing free surface. Free surfaces can result from contamination during the line fabrication process, which hinders the bounding of the surrounding layer to the metal surface. Assuming a circular flaw of radius R_p, the critical stress for void nucleation becomes [35]

$$\sigma_{th} = \frac{2\gamma_s}{R_p}, \tag{68}$$

where γ_s is the surface free energy of the metal.

Clemens et al. [66] showed that the above equation is valid as long as the void grows in the contaminated region. However, it is possible that the void extends beyond the flaw area, as shown by Fig. 11, once the equilibrium contact angle, θ_c, is reached. This equilibrium contact angle is determined by the interfacial energy balance and lies in the range $0 < \theta_c < 90^\circ$. In this case, the threshold stress is given by [36,66]

$$\sigma_{th} = \frac{2\gamma_s \sin\theta_c}{R_p}, \tag{69}$$

which may represent a small decrease in the nucleation energy barrier.

The critical stress is significantly reduced as the flaw area increases. For instance, for a flaw radius as small as 10 nm we obtain $\sigma_{th} \approx 340$ MPa [45], which can be certainly reached by thermal stresses alone. If we consider that the contaminated region can extend trough the whole line width, for a line 100 nm wide we get $\sigma_{th} \approx 70$ MPa. Such a stress magnitude is quite low and can be easily obtained in an interconnect line under electromigration.

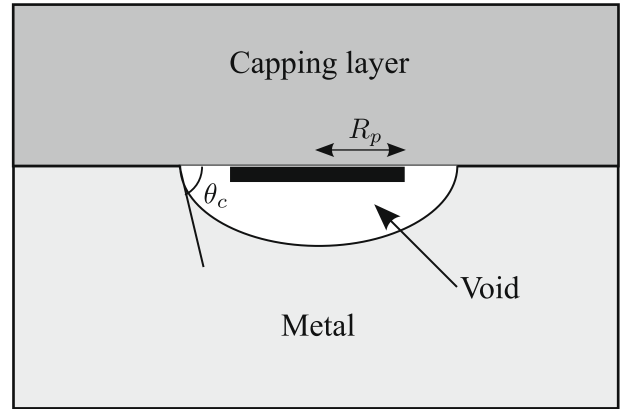

Fig. 11. Schematic void nucleation at an interface site of weak adhesion according to Clemens et al. [66] and Gleixner et al. [36].

7. Void evolution

The development of fatal voids, i.e. voids that trigger the line failure is the ultimate cause for the electromigration induced interconnect failure [67,68]. The failure criterion is typically set as a maximum resistance increase that is tolerated for the corresponding interconnect line. Once a void is nucleated it can evolve, until it causes a significant resistance increase or even completely severs the line.

The void evolution phase can encompass several processes: a void can migrate along the interconnect [52,55], interact with the local microstructure [55,69,70] and grow, or even heal [55,71], undergo morphologic changes, assuming wedge-like shape or slit-like shape [58], before it definitely triggers interconnect failure. Furthermore, multiple voids can form in a line, so that their migration and agglomeration at a specific critical site can be the mechanism responsible for the interconnect failure [52–54].

The void surface acts as an additional path for atomic migration. The chemical potential of an atom on the void surface is given by [21,72,73]

$$\mu_s = \mu_0 + \Omega(w - \gamma_s\kappa), \tag{70}$$

where μ_0 is a reference chemical potential, $w = \boldsymbol{\sigma} : \boldsymbol{\varepsilon}/2$ is the elastic energy density of the material adjacent to the void, γ_s is the surface free energy and κ is the curvature of the void surface. Thus, the atomic flux along the void surface due to gradients in chemical potential plus electromigration has the form

$$\vec{J}_s = -\frac{D_s\delta_s}{kT}(\nabla_s\mu_s + e|Z^*|\vec{E}_s) \tag{71}$$

where D_s is the surface diffusivity, δ_s is the surface thickness, $\vec{E}_s$ is the electric field tangential to the void surface, and ∇_s denotes the gradient along the surface. By mass conservation the normal velocity at any point on the surface is given by [72,73]

$$v_n = -\nabla_s \cdot \vec{J}_s. \tag{72}$$

Void evolution due to electromigration is a complex dynamic process, for which modeling is a challenging task and, moreover, represents a moving boundary problem. Analytical solutions can only describe the asymptotic behavior of the moving boundary [61,74–79], since, in general, the shape changes which the void experiences

cannot be analytically resolved. Therefore, a more general treatment demands the application of numerical methods and special techniques for tracking the void. Below we present some major contributions to void evolution modeling and associated numerical methods.

7.1. Sharp interface models

Arzt et al. [80] and Kraft and Arzt [81] neglected the effect of elastic energy and considered a two-dimensional case, so that (71) becomes

$$J_s = \frac{D_s\delta_s}{kT}\left(\Omega\gamma_s\frac{\partial\kappa}{\partial s} - e|Z^*|\rho j_s\right) \tag{73}$$

where j_s is the surface component of the current density. Thus, the surface velocity can be written as

$$v_n = -\frac{D_s\delta_s}{kT}\frac{\partial}{\partial s}\left(\Omega\gamma_s\frac{\partial\kappa}{\partial s} - e|Z^*|\rho j_s\right). \tag{74}$$

Void evolution is simulated by a numerical scheme which combines the finite element method (FEM) and the finite difference method (FDM). FEM is used to obtain the temperature and current density distribution in the vicinity of a void in a finite line. These results are used to solve the void motion equation, (74), by FDM. Then, the new void shape is remeshed. This procedure is iterated several times in order to describe the whole void evolution process and obtain the final void shape [81].

In such an approach there is no exchange flux between the void with its surrounding. Consequently, the void shape changes, but it cannot grow and its volume remains constant. Kraft and Arzt overcame this problem by introducing an artificial growth rate after the FD calculation and before the remeshing procedure [81]. They found out that shape change is triggered as the void spans about half of the line width, as shown in Fig. 12. Moreover, it depends on the growth rate, in such a way that lower growth rates tend to lead to slit-like voids, while higher growth rates tend to yield wedge-shaped voids.

Fridline and Bower [82] applied a similar model, but introduced an anisotropic diffusion coefficient of the form

$$D_s(\theta,T) = D_0(T)\{1 + m[1 - \cos(n\theta - \theta_0)]\}, \tag{75}$$

where θ is the angle between the tangent to the void surface and the current direction, m determines the degree of anisotropy, n determines the crystallographic symmetry, and θ_0 represents the orientation of the line with respect to the crystal planes. The model is solved by a two-step FEM, where first the voltage distribution is calculated, followed by the solution of the surface motion equation. Also, a remeshing procedure is continuously applied using an advancing front algorithm as the void changes its shape [82]. It was shown that even a small anisotropy in surface diffusivity can lead to a large shape change of the void and that the crystal orientation with respect to the line direction is an important factor regarding the void shape and evolution tendency, as depicted in Fig. 13.

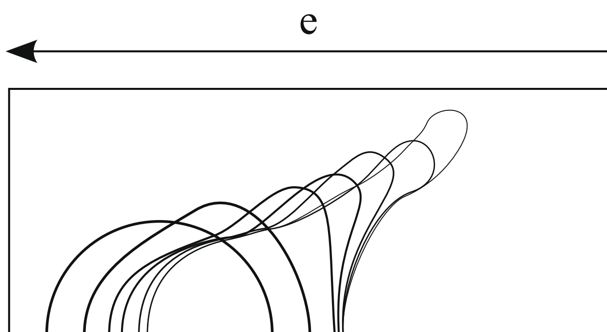

Fig. 12. Void shape change is triggered as it spans about half of the line width [81].

The models above were further developed by Xia et al. [83], who took also into account the effects of mechanical stress on the void evolution. The normal velocity of the surface of the void is written in two-dimensions as

$$v_n = -\frac{D_s\delta_s}{kT}\left(-\Omega\frac{\partial^2 w}{\partial s^2} + \Omega\gamma_s\frac{\partial^2\kappa}{\partial s^2} + e|Z^*|\frac{\partial\varphi}{\partial s}\right), \tag{76}$$

where the electromigration term is expressed through the electric potential φ. The calculation of the elastic energy density is performed by solving the mechanical Eqs. (56)–(58). A FEM approach using adaptive mesh generation and an advancing front algorithm to track the void evolution is applied.

Xia et al. showed that the void remains circular and migrates along the line, if the surface energy prevails. However, if the driving force associated to electromigration and/or the elastic strain energy dominate over the surface energy, the void tends to collapse into a slit or to break down into smaller voids. Therefore, electromigration and elastic strain energy gradients act in a cooperative manner, promoting void instability. Fig. 14 shows the

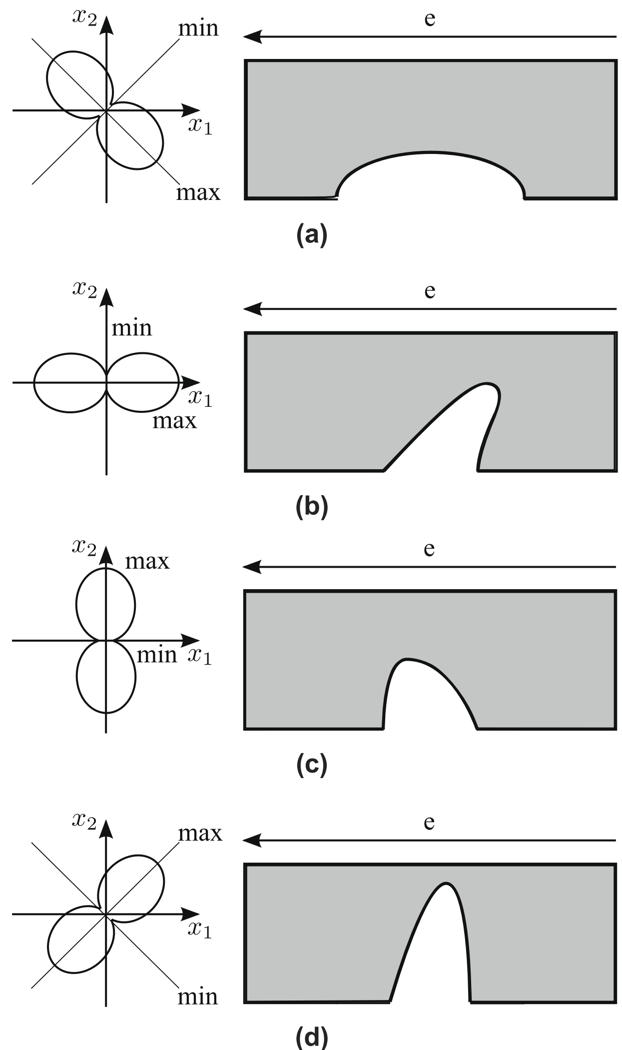

Fig. 13. Void shape for different crystal orientations [82]. (a) $\theta_0 = \pi/2$, (b) $\theta_0 = \pi$, (c) $\theta_0 = 0$, (d) $\theta_0 = 3\pi/2$.

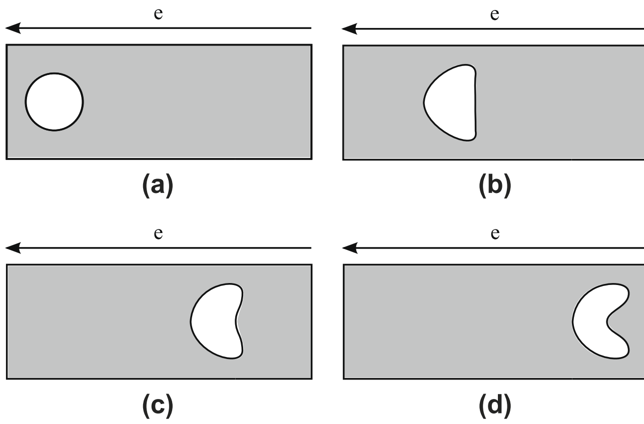

Fig. 14. Void evolution due to stress and electric field for $\chi = 10$ and $\Lambda = 0.1$ [83].

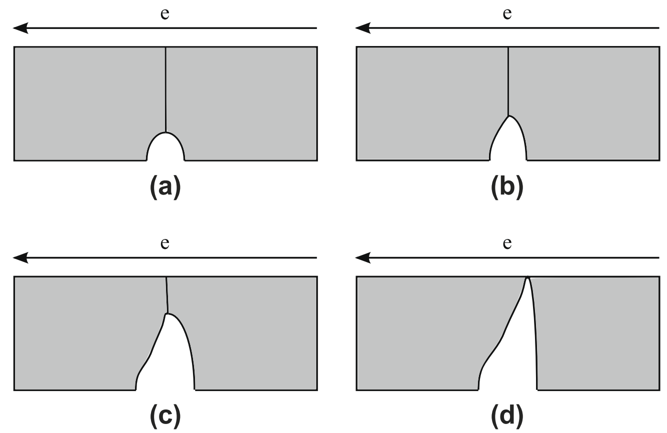

Fig. 15. Void growing along a grain boundary due to flux divergences [85].

development of such an instability. The same results were obtained with three-dimensional simulation performed by Zhang et al. [84], who used essentially the same model and numerical approach.

These effects can be described by considering the dimensionless quantities [75–77]

$$\chi = \frac{e|Z^*|E_\infty r_0^2}{\Omega\gamma_s}, \tag{77}$$

$$\Lambda = \frac{\sigma^2 r_0}{E\gamma_s}, \tag{78}$$

where r_0 is the initial radius of the void, E_∞ is the electric field applied in the line, σ is the applied stress, and E is Young's modulus. The above equations represent a relative measure of the influence of the driving forces on the void evolution, and the competition between them dictates the direction of void development. Small values indicate that the surface energy term dominates, so that the void tends to be stable and relax to a rounded shape. On the other hand, when the quantities above become large, the electromigration and/or the elastic energy gradient term dictates the void evolution in such a way that the void tends to collapse into a slit-like shape. Thus, there is a critical χ_c and Λ_c so that for $\chi < \chi_c$ and $\Lambda < \Lambda_c$ the void remains rounded, and for $\chi > \chi_c$ or $\Lambda > \Lambda_c$ the void can collapse into a slit [75–77].

A significant improvement in the capabilities of void evolution simulation was carried out by Bower and Shankar [85]. In their model the interaction between the void with its local surrounding is also included, so that exchange fluxes between grain boundaries, or interfaces, with the void are considered. Thus, the model includes the effects of grain boundary diffusion, grain boundary sliding and migration, as well as surface diffusion. Bower and Shankar showed that a void de-pins from the grain boundary, when the surface evolves much faster than the grain boundary. On the other hand, if the surface and the grain boundary migrate at similar rates the void remains pinned at the grain boundary. Fig. 15 shows a void growing along the grain boundary. Void growth takes place due to existent flux divergences at grain boundary triple points or at surfaces connected to the void [85].

The common drawback of these models is that they all use finite difference or finite element schemes, which require a continuous explicit void surface tracking and, consequently, a continuous remeshing and interpolation procedure. This approach is quite complicated to implement and computationally very demanding. Therefore, it can be satisfactorily applied only for two-dimensional cases and cannot be further extended.

7.2. Diffuse interface model

The shortcoming of the sharp interface models were overcome by Mahadevan and Bradley [86,87] with the application of the so-called phase field or diffuse interface model. The main advantage of this method is that the void surface is implicitly represented by a field parameter. In this way, void evolution is described by the evolution of the field parameter, so that explicit surface tracking is not needed.

The field parameter, ϕ, separates the void phase from the solid phase. It assumes a value $\phi = +1$ in the solid phase, $\phi = -1$ in the void phase, and varies over a narrow interfacial layer between the solid and void surface, $-1 < \phi < +1$. Defining the free energy of the line as a functional $F(\phi, \nabla\phi, \boldsymbol{\varepsilon})$, the chemical potential is expressed in the form [88]

$$\mu = \frac{\delta F}{\delta \phi}. \tag{79}$$

Using (79), Eq. (71) can be expressed as $\vec{J}_s = \vec{J}_s(\phi)$ and the evolution of the field parameter is governed by a Cahn–Hilliard equation of the form [88]

$$\frac{\partial \phi}{\partial t} = -\nabla \cdot \vec{J}_s(\phi). \tag{80}$$

A thorough implementation of this method for two-dimensional simulations was carried out by Bhate et al. [72,73,89]. All driving forces for atomic migration are included in the modeling and, moreover, a slight modification of (80), given by

$$\frac{\partial \phi}{\partial t} = -\nabla \cdot \vec{J}_s(\phi) + G, \tag{81}$$

is employed, where G accounts for the exchange flux between the bulk and the void surface.

Eq. (81) is numerically solved using an implicit finite element scheme, together with the associated mechanical and electrical equations. In order to adequately describe the order parameter in the narrow interfacial layer surrounding the void phase Bhate et al. use hierarchically structured meshes. The order parameter equation is solved on a finer mesh which is obtained by refinement of a coarser mesh, the latter employed for the electrical and mechanical calculations [72,73,89]. The aforementioned meshes are static in the entire simulation domain, and they are stored during the whole simulation cycle.

Another implementation of the diffuse interface model was performed by Ceric et al. [90–92]. In their implementation electromigration and surface curvature gradients are taken into account, while the elastic strain energy term is neglected. As in the work

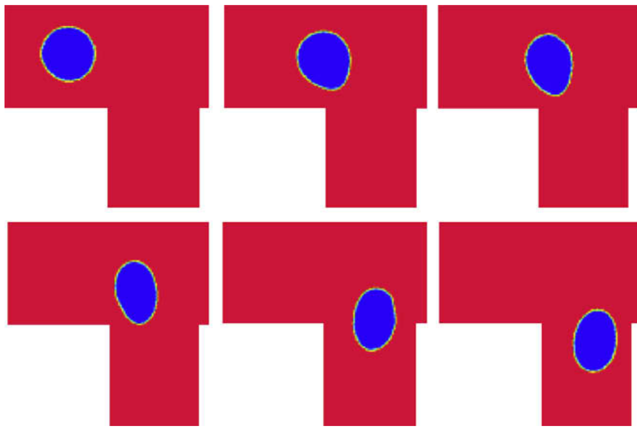

Fig. 16. Void migration and shape change driven by electromigration [90].

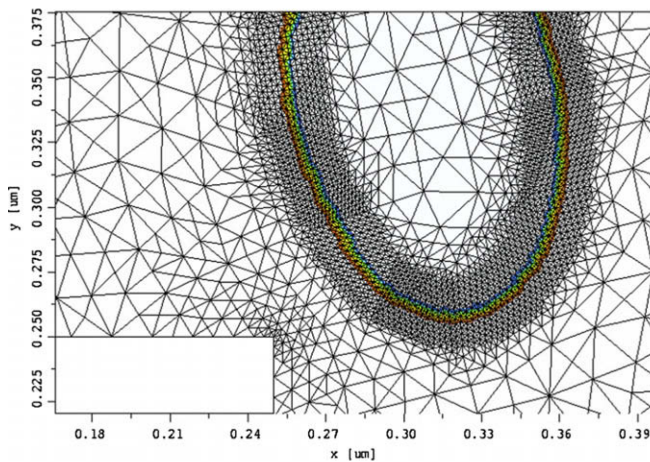

Fig. 17. Adaptive mesh procedure refines the mesh around the void surface, in such a way that high resolution for the order parameter can be obtained [90].

of Bhate et al. [72,73], Ceric et al. used a FEM scheme for solving the Cahn–Hilliard equation. Fig. 16 shows void migration accompanied by a slight shape change in a two-dimensional via structure.

Differently from Bhate's method, Ceric's numerical approach implements an adaptive mesh algorithm to generate a fine mesh area around the void surface and a coarse mesh at locations where high resolution of the order parameter is not needed. This is depicted in Fig. 17. The local refinement allows regions of high curvature and high gradients to be properly resolved. However, the adaptive mesh procedure is prohibitively demanding for three-dimensional simulations.

The main advantage of the diffuse interface model is that the implicit description of the void surface may avoid surface tracking procedures. Moreover, the consideration of surface and elastic strain energy in the model is straightforward, and boundary conditions can be automatically incorporated into the scheme without the need to be enforced at the void surface. The main drawback is that a very fine mesh is needed around the void in order to adequately describe the field parameter at the narrow interfacial layer between the void and the metal. The result is an increased complexity for the numerical implementation.

7.3. Level set method

Another method which has appeared as possible solution for three-dimensional implementations is the Level Set Method (LSM) [93]. In microelectronics the level set method has been mostly applied for topography simulations, like etching and deposition processes [94,95]. In this method the void surface, Γ, is implicitly represented by the level set of a given function,

$$\Gamma = \{\vec{r}|\phi(\vec{r}) = c\}, \tag{82}$$

for a given constant c. Void evolution is described by a Hamilton–Jacobi equation,

$$\frac{\partial\phi}{\partial t} + v_n\|\nabla\phi\| = 0, \tag{83}$$

where ϕ represents the level set function and v_n is the normal surface velocity. The velocity field accounts for the physical effects acting on the moving boundary, as given by (72), and dictates the evolution of the level set.

A level set formulation for two-dimensional grain boundary grooving due to surface diffusion driven by electromigration and local curvature gradients was proposed by Khenner et al. [96,97]. Based on these works, Nathan et al. [98] carried out numerical simulations of electromigration drift velocity, given by an Arrhenius expression,

$$v_d = v_0 \exp\left(-\frac{E_a}{kT}\right), \tag{84}$$

and showed that the simulated drift velocities were in excellent agreement with experimental results.

Using a similar approach Averbuch et al. [99] simulated void evolution under curvature gradients and electromigration forces, as given by (74), for several initial void shapes, like elliptic, triangular, and square voids. The level set equation, (83), was solved using a finite difference discretization on a regular grid and a second-order Runge–Kutta time integration scheme [96,97,99]. It was shown that under weak electric fields an arbitrary initial shape becomes circular and the void migrates in the direction of the applied electric field. For strong electric fields the circular void becomes unstable and it evolves to slit-like shapes. These results are similar to those obtained by Xia et al. [83].

Cacho et al. [100] describe a two-dimensional void surface by

$$\Gamma = \left\{x, y|\phi(x, y) = \frac{1}{2}\right\}, \tag{85}$$

where $\phi = 1$ in the metal and $\phi = 0$ in the void. Since the normal velocity given by (74) does not consider mass exchange between the void and the metal line, the authors redefine the surface flux as

$$\vec{J}_s = -\frac{D_v C_v}{kT}(\Omega\gamma_s\nabla_s\kappa + e|Z^*|\nabla_s\varphi), \tag{86}$$

where $\vec{J}_s$ here refers to a vacancy flux. The vacancy diffusion coefficient is expressed as

$$D_v = \delta(\phi)D_s + \phi D_v^b, \tag{87}$$

where $\delta(\phi)$ is a smooth function of ϕ, D_s represents the vacancy diffusivity at the void surface, and D_v^b is the vacancy diffusivity in the bulk. With these modifications the vacancy continuity equation, (8), becomes

$$\frac{\partial C_v}{\partial t} = -\phi\nabla\cdot\vec{J}_v - \delta(\phi)\nabla_s\cdot\vec{J}_s + \phi G, \tag{88}$$

where $\vec{J}_v$ is given by (7). In the metal bulk, $\phi = 1$ and $\delta(\phi) = 0$, and the equation above reduces to the usual continuity equation, (8). At the same time $\phi = 0$ and $\delta(\phi) = 0$ in the void, so that the equation reproduces the surface velocity, (72). Thus, Cacho et al. express the normal velocity as

$$v_n = -\text{sign}(N - N_0)K\left|\frac{\partial N}{\partial t}\right|, \tag{89}$$

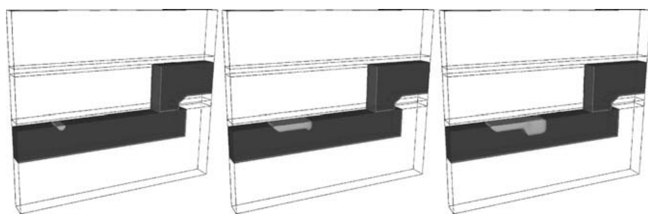

Fig. 18. Three-dimensional void evolution under electromigration in the presence of grain boundaries [101].

where $N = C_v/C_{v0}, N_0$ is a given critical vacancy concentration, and K is a constant.

Recently, Ceric et al. [101] studied void evolution under the influence of electromigration and the surface energy gradient using the level set method for three-dimensional simulations. Initially, a void is considered to nucleate at a junction between a grain boundary and the copper/capping layer interface which is a natural free adhesion patch. The void then moves in the direction of the current flow, until a second grain boundary is reached. The grain boundary acts as a fast diffusivity path. Thus, an additional incoming flux of vacancies from the grain boundary leads to void growth through the line thickness and further shape change. This void evolution process is shown by Fig. 18. This simulation result demonstrate a decisive impact of the microstructure on the void evolution mechanisms and, consequently, failure development [101].

The level set method is a powerful method for simulating moving boundary problems, offering the advantage that the moving boundary can be implicitly represented, in such a way that surface tracking is avoided. Several algorithms for level set calculations have been proposed [102–104]. The level set equation is typically solved on rectangular grids, which may be a limitation for simulation of general complex structures. However, some works have been recently published where the level set method is implemented for unstructured triangulated meshes in connection to mass transport and mechanics [105–107].

8. Summary and outlook

We discussed a wide variety of electromigrations models which have been proposed since the electromigration phenomenon was first identified. We started from the early basic derivation of Black's equation and gradually presented the development of the models as they became more and more complete. It is clear that electromigration modeling is a rather complex and challenging task. The models for the nucleation phase have successfully incorporated a wide variety of physical effects on the material transport equations in connection with mechanics, like the influence of microstructure and material interfaces acting not only as fast diffusivity paths, but also as sites for vacancy annihilation and generation, for fully three-dimensional cases. This allowed the prediction of the stress build-up in an interconnect line and to explain several experimental observations regarding the preferable nucleation sites and void nucleation conditions. In turn, the void evolution models have enabled to track void growth and shape changes in an interconnect, relating the void development mechanisms to the stress conditions at which the line is subjected to and, moreover, to the local line structure and properties. We showed that different numerical approaches have been used for the void evolution phase. The main difficulty here is that the void surface has to be "tracked" as the void evolves. This requires special numerical techniques and algorithms. The diffuse interface model and level set method appear to be best suited, since the void is implicitly represented, therefore, avoiding the prohibitively demanding explicit surface tracking procedures.

To sum up, physical electromigration modeling has allowed to interpret several experimental observations. On the other hand, we feel the connection of numerical simulations performed by the available tools to lifetime extrapolation and to lifetime statistical distribution is currently loose. Improvements in this area is of crucial importance for a sound reliability prediction of metallizations for the next technological nodes.

Acknowledgment

Support by the Austrian Science Fund (FWF) with Project P18825-N14 is gratefully acknowledged.

References

[1] International Technology Roadmap for Semiconductors; 2008.
[2] Black JR. Mass transport of aluminum by momentum exchange with conducting electrons. Proc 6th Ann Reliab Phys Symp 1967:148–59.
[3] Black JR. Electromigration – a brief survey and some recent results. IEEE Trans Electron Devices 1969;16(4):338–47.
[4] Black JR. Electromigration failure modes in aluminum metallization for semiconductor devices. Proc IEEE Lett 1969;57(9):1578–94.
[5] Blair JC, Ghate PG, Haywood CT. Concerning electromigration in thin films. Proc IEEE Lett 1971;59:1023–4.
[6] Huntington HB, Grone AR. Current-induced marker motion in gold wires. J Phys Chem Solids 1961;20(1):76–87.
[7] Hofman GL, Breitling HM. On the current density dependence of electromigration in thin films. Proc IEEE Lett 1970;58:833.
[8] Shatzkes M, Lloyd J. A model for conductor failure considering diffusion concurrently with electromigration resulting in a current exponent of 2. J Appl Phys 1986;59(11):3890–3.
[9] Lloyd J. Electromigration failure. J Appl Phys 1991;69(11):7601–4.
[10] Kirchheim R, Kaeber U. Atomistic and computer modeling of metallization failure of integrated circuits by electromigration. J Appl Phys 1991;70(1):172–81.
[11] Kirchheim R. Stress and electromigration in Al-lines of integrated circuits. Acta Metall Mater 1992;40(2):309–23.
[12] Korhonen MA, Borgesen P, Tu KN, Li C-Y. Stress evolution due to electromigration in confined metal lines. J Appl Phys 1993;73(8):3790–9.
[13] Clement JJ, Thompson CV. Modeling electromigration-induced stress evolution in confined metal lines. J Appl Phys 1995;78(2):900–4.
[14] Lloyd JR. Black's law revisited – nucleation and growth in electromigration failure. Microelectron Reliab 2007;47:1468–72.
[15] de Groot SR. Theorie phenomenologique de L'Effet soret. Physica 1942:699–707.
[16] Sukharev V, Zschech E, Nix WD. A model for electromigration-induced degradation mechanisms in dual-inlaid copper interconnects: effect of microstructure. J Appl Phys 2007;102:053505.
[17] Liniger EG, Gignac LM, Hu C-K, Kaldor S. In situ study of void growth kinetics in electroplated Cu lines. J Appl Phys 2002;92(4):1803–10.
[18] Lodder A, Dekker JP. The electromigration force in metallic bulk. AIP Conf Proc 1998;418:315–29.
[19] Rosenberg R, Ohring M. Void formation and growth during electromigration in thin films. J Appl Phys 1971;42(13):5671–9.
[20] Attardo MJ, Rosenberg R. Electromigration damage in aluminum film conductors. J Appl Phys 1970;41(6):2381–6.
[21] Mullins WW. Mass transport at interfaces in single component systems. Metall Mater Trans A 1995;26:1918–29.
[22] Blech IA. Electromigration in thin aluminum films on titanium nitride. J Appl Phys 1976;47(4):1203–8.
[23] Blech IA, Herring C. Stress generation by electromigration. Appl Phys Lett 1976;29(3):131–3.
[24] Blech IA, Tai KL. Measurement of stress gradients generated by electromigration. Appl Phys Lett 1977;30(8):387–9.
[25] Herring C. Diffusional viscosity of a polycrystalline solid. J Appl Phys 1950;21:437–45.
[26] Ogawa ET, Bierwag AJ, Lee K-D, Matsuhashi H, Justinson PR, et al. Direct observation of a critical length effect in dual-damascene Cu/oxide interconnects. Appl Phys Lett 2001;78(18). 2645–2652.
[27] Ney D, Federspiel X, Girault V, Thomas O, Gergaud P. Stress-induced electromigration backflow effect in copper interconnects. Trans Device Mater Reliab 2006;6(2):175–80.
[28] Doyen L, Petitprez E, Waltz P, Federspiel X, Arnaud L, Wouters Y. Extensive analysis of resistance evolution due to electromigration induced degradation. J Appl Phys 2008;104:123521.
[29] Oates AS, Lin MH. Void nucleation and growth contributions to the critical current density for failure in Cu vias. Proc Intl Reliab Phys Symp 2009:452–6.
[30] Lloyd JR. Electromigration and mechanical stress. Microelectron Eng 1999;49:51–64.
[31] Balluffi RW, Granato AV. Dislocations, vacancies and interstitials. In: Nabarro FNR (Ed.), Dislocation in solids; 1979. p. 1–133.

[32] Clement JJ. Reliability analysis for encapsulated interconnect lines under DC and pulsed DC current using a continuum electromigration transport model. J. Appl. Phys. 1997;82(12):5991–6000.
[33] Shewmon PG. Diffusion in solids. New York: McGraw-Hill; 1963.
[34] Carslaw HS, Jaeger JC. Conduction of heat in solids. Oxford: Clarendon Press; 1947.
[35] Flinn PA. Mechanical stress in VLSI interconnections: origins, effects, measurement, and modeling. MRS Bull 1995:70–3.
[36] Gleixner RJ, Clemens BM, Nix WD. Void nucleation in passivated interconnect lines: effects of site geometries, interfaces, and interface, flaws. J Mater Res 1997;12:2081–90.
[37] Ye H, Basaran C, Hopkins DC. Numerical simulation of stress evolution during electromigration in IC interconnect lines. IEEE Trans Components Pack Technol 2003;26(3):673–81.
[38] Lin M, Basaran C. Electromigration induced stress analysis using fully coupled mechanical-diffusion equations with nonlinear material properties. Comput Mater Sci 2005;34:82–98.
[39] Basaran C, Lin M. Damage mechanics of electromigration in microelectronics copper interconnects. Int J Mater Struct Integrity 2007;1:16–39.
[40] Sukharev V, Choudhury R, Park CW. Physically-based simulation of the early and long-term failures in copper dual-damascene interconnects. Proc Intl Integrated Reliab Workshop 2003:80–5.
[41] Sukharev V, Zschech E. A model for electromigration-induced degradation mechanisms in dual-inlaid copper interconnects: effect of interface bonding strength. J Appl Phys 2004;96(11):6337–43.
[42] Sukharev V. Physically based simulation of electromigration-induced degradation mechanisms in dual-damascene copper interconnects. ieeecadics 2005;24(9):1326–35.
[43] Dalleau D, Weide-Zaage K. Three-dimensional voids simulation in chip metallization structures: a contribution to reliability evaluation. Microelectron Reliab 2001;41:1625–30.
[44] Dalleau D, Weide-Zaage K, Danto Y. Simulation of time depending void formation in copper, aluminum and tungsten plugged via metallization structures. Microelectron Reliab 2003;43:1821–6.
[45] Ceric H, de Orio RL, Cervenka J, Selberherr S. A comprehensive TCAD approach for assessing electromigration reliability of modern interconnects. IEEE Trans Mater Device Reliab 2009;9(1):9–19.
[46] Meyer MA, Herrmann M, Langer E, Zschech E. In situ SEM observation of electromigration phenomena in fully embedded copper interconnect structures. Microelectron Eng 2002;64:375–82.
[47] Povirk GL. Numerical simulations of electromigration and stress-driven diffusion in polycrystalline interconnects. Mater Res Soc Symp Proc 1997;473:337–42.
[48] Rzepka S, Korhonen MA, Weber ER, Li C-Y. Three-dimensional finite element simulation of electro and stress migration effects in interconnect lines. Mater Res Soc Symp Proc 1997;473:329–35.
[49] Sarychev ME, Zhitnikov YV, Borucki L, Liu C-L, Makhviladze TM. General model for mechanical stress evolution during electromigration. J Appl Phys 1999;86(6):3068–75.
[50] Goldstein RV, Sarychev ME, Shirabaikin DB, Vladimirov AS, Zhitnikov YV. Modeling electromigration and the void nucleation in thin-film interconnects of integrated circuits. Int J Fract 2001;109:91–121.
[51] Lau F, Mazure C, Werner C, Orlowski M. A model for phosphorus segregation at the silicon–silicon dioxide interface. Appl Phys A 1989;49:671–5.
[52] Vairagar AV, Mhaisalkar SG, Krishnamoorthy A. Electromigration behavior of dual-damascene Cu interconnects – structure, width, and length dependences. Microelectron Reliab 2004;44:747–54.
[53] Vairagar AV, Mhaisalkar SG, Krishnamoorthy A, Tu KN, Gusak AM, Meyer MA, et al. In situ observation of electromigration-induced void migration in dual-damascene Cu interconnect structures. Appl Phys Lett 2004;85(13):2502–4.
[54] Vairagar AV, Mhaisalkar SG, Meyer MA, Zschech E, Krishnamoorthy A, Tu KN, et al. Direct evidence of electromigration failure mechanism in dual-damascene Cu interconnect tree structures. Appl Phys Lett 2005;87:081909.
[55] Choi ZS, Mönig R, Thompson CV. Effects of microstructure on the formation, shape, and motion of voids during electromigration in passivated copper interconnects. J Mater Res 2008;23(2):383–91.
[56] Sukharev V, Zschech E. Microstructure effect on EM-induced copper interconnect degradation: experiment and simulation. Microelectron Eng 2005;82:629–38.
[57] Zschech E, Engelmann HJ, Meyer MA, Kahlert V, Vairagar AV, Mhaisalkar SG, et al. Effect of interface strength on electromigrationinduced inlaid copper interconnect degradation: experiment and simulation. Z Metallkd 2005; 96(9):966–71.
[58] Yan MY, Suh JO, Ren F, Tu KN, Vairagar AV, Mhaisalkar SG, et al. Effect of Cu_3Sn coatings on electromigration lifetime improvement of Cu dual-damascene interconnects. Appl Phys Lett 2005;87:211103.
[59] Marcoux PJ, Merchant PP, Naroditsky V, Rehder WD. A new 2d simulation model of electromigration. Hewlett–Packard J 1989:79–84.
[60] Clement JJ, Lloyd JR. Numerical investigations of the electromigration boundary value problem. J Appl Phys 1992;71(4):1729–31.
[61] Nix WD, Arzt E. On void nucleation and growth in metal interconnect lines under electromigration conditions. Metall Trans A 1992;23:2007–13.
[62] Hull D, Rimmer DE. The growth of grain–boundary voids under stress. Philos Mag 1959;4:673–87.
[63] Harris JE. Nucleation of creep cavities in magnesium. Trans Met AIME 1965;233:1509–16.
[64] Raj R, Ashby MF. Intergranular fracture at elevated temperatures. Acta Metall 1975;23:653–66.
[65] Hirth JP, Nix WD. Analysis of cavity nucleation in solids subjected to external and internal stresses. Acta Metall 1985;33:359–68.
[66] Clemens BM, Gleixner RJ, Nix WD. Void nucleation on a contaminated patch. J Mater Res 1997;12:2038–42.
[67] Doyen L, Petitprez E, Waltz P, Federspiel X, Arnaud L, Wouters Y. Extensive analysis of resistance evolution due to electromigration-induced degradation. J Appl Phys 2008;104:123521.
[68] Hauschildt M, Gall M, Thrasher S, Justison P, Hernandez R, Kawasaki H, et al. Statistical analysis of electromigration lifetimes and void evolution. J Appl Phys 2007;101:043523.
[69] Arnaud L, Berger T, Reimbold G. Evidence of grain-boundary versus interface diffusion in electromigration experiments in copper damascene interconnects. J Appl Phys 2003;93(1):192–204.
[70] Choi ZS, Mönig R, Thompson CV. Dependence of the electromigration flux on the crystallographic orientations of different grains in polycrystalline copper interconnects. Appl Phys Lett 2007;90:241913.
[71] Besser PR, Madden MC, Flinn PA. In situ scanning electron microscopy observation of the dynamic behavior of electromigration voids in passivated aluminum lines. J Appl Phys 1992;72(8):3792–7.
[72] Bhate DN, Kumar A, Bower AF. Diffuse interface model for electromigration and stress voiding. J Appl Phys 2000;87(4):1712–21.
[73] Bhate DN, Bower AF, Kumar A. A phase field model for failure in interconnect lines due to coupled diffusion mechanisms. J Mech Phys Solids 2002;50:2057–83.
[74] Ho PS. Motion of inclusion induced by a direct current and a temperature gradient. J Appl Phys 1970;41(1):64–8.
[75] Suo Z, Wang W, Yang M. Electromigration instability: transgranular slits in interconnects. Appl Phys Lett 1994;64(15):1944–6.
[76] Suo Z, Wang W. Diffusive void bifurcation in stressed solid. J Appl Phys 1994;76(6):3410–21.
[77] Wang W, Suo Z, Hao T-H. A simulation of electromigration-induced transgranular slits. J Appl Phys 1996;79(5):2394–403.
[78] Zaporozhets TV, Gusak AM, Tu KN, Mhaisalkar SG. Diffuse interface model for electromigration and stress voiding. J Appl Phys 2005;98:103508.
[79] Castro DT, Hoofman RJO, Michelon J, Gravesteijn DJ, Bruynseraede C. Void growth modeling upon electromigration stressing in narrow copper lines. J Appl Phys 2007;102:123515.
[80] Arzt E, Kraft O, Nix WD, Sanchez JJE. Electromigration failure by shape change of voids in bamboo lines. J Appl Phys 1994;76(3):1563–71.
[81] Kraft O, Arzt E. Electromigration mechanisms in conductor lines: void shape changes and slit-like failure. Acta Mater 1997;45(4):1599–611.
[82] Fridline DR, Bower AF. Influence of anisotropic surface diffusivity on electromigration induced void migration and evolution. J Appl Phys 1999;85(6):3168–74.
[83] Xia L, Bower AF, Suo Z, Shih CF. A finite element analysis of the motion and evolution of voids due to strain and electromigration induced surface diffusion. J Mech Phys Solids 1997;45(9):1473–93.
[84] Zhang YW, Bower AF, Xia L, Shih CF. Three dimensional finite element analysis of the evolution of voids and thin films by strain and electromigration induced surface diffusion. J Mech Phys Solids 1999;47:173–99.
[85] Bower AF, Shankar S. Finite element model of electromigration induced void nucleation, growth and evolution in interconnects. Modell Simul Mater Sci Eng 2007;15:923–40.
[86] Mahadevan M, Bradley RM. Simulations and theory of electromigration-induced slit formation in unpassivated single-crystal metal lines. Phys Rev B 1999;59(16):11037–46.
[87] Mahadevan M, Bradley RM. Phase field model of surface electromigration in single crystal metal thin films. Physica D 1999;126:201–13.
[88] Gurtin ME. Generalized Ginzburg–Landau and Cahn–Hilliard equations based on a microforce balance. Physica D 1996;92:178–92.
[89] Bhate DN. Diffuse interface model of void growth and migration in microelectronic interconnect lines. Dissertation, Brown University; 2001.
[90] Ceric H, Selberherr S. An adaptive grid approach for the simulation of electromigration induced void migration. IEICE Trans Electron 2002:421–6.
[91] Ceric H, Selberherr S. Simulative prediction of the resistance change due to electromigration induced void evolution. Microelectron Reliab 2002;42:1457–60.
[92] Ceric H, Sabelka R, Holzer S, Wessner W, Wagner S, Grasser T, et al. The evolution of the resistance and current density during electromigration. Proc Simul Semicond Process Devices 2004:331–4.
[93] Sethian JA. Level set methods and fast marching methods: evolving interfaces in computational geometry, fluid mechanics, computer vision and materials science. Cambridge University Press; 1999.
[94] Ertl O, Selberherr S. A fast level set framework for large three-dimensional topography simulations. Comput Phys Commun 2009;180:1242–50.
[95] Ertl O, Selberherr S. Three-dimensional level set based bosch process simulations using ray tracing for flux calculation. Microelectron Eng 2010;87:20–9.
[96] Khenner M, Averbuch A, Israeli M, Nathan M, Glickman E. Level set modeling of transient electromigration grooving. Comput Mater Sci 2001;20:235–50.
[97] Khenner M, Averbuch A, Israeli M, Nathan M. Numerical simulation of grain-boundary grooving by level set method. J Comp Phys 2001;170:764–84.

[98] Nathan M, Glickman E, Khenner M, Averbuch A, Israeli M. Electromigration drift velocity in Cu interconnects modeled with the level set method. Appl Phys Lett 2000;77(21):3355–7.
[99] Averbuch A, Israeli M, Ravve I, Yavneh I. Computation for electromigration in interconnects of microelectronic devices. J Comp Phys 2001;167:316–71.
[100] Cacho F, Fiori V, Doyen L, Chappaz C, Tavernier C, Jaouen H. Electromigration induced failure mechanism: multiphysics model and correlation with experiments. Proc EuroSimE 2008:1–6.
[101] Ceric H, de Orio RL, Cervenka J, Selberherr S. Copper microstructure impact on evolution of electromigration induced voids. Proc Intl Conf Simul Semicond Process Devices (SISPAD) 2009:178–81.
[102] Adalsteinsson D, Sethian JA. A fast level set method for propagating interfaces. J Comput Phys 1995;118:269–77.
[103] Whitaker RT. A level-set approach to 3d reconstruction from range data. Int J Comput Vis 1998;29(3):203–31.
[104] Houston B, Nielsen MB, Batty B, Nilsson O, Museth K. Hierarchical RLE level set: a compact and versatile deformable surface representation. ACM Trans Graph 2006;25(1):151–75.
[105] Barth TJ, Sethian JA. Numerical schemes for the Hamilton–Jacobi and level set equations on triangulated domains. J Comput Phys 1998;145:1–40.
[106] Mourad HM, Dolbow J, Garikipati K. An assumed-gradient finite element method for the level set equation. Int J Numer Methods Eng 2005;64:1009–32.
[107] Mourad HM, Dolbow J, Garikipati K. Advances in the numerical treatment of grain-boundary migration: coupling with mass transport and mechanics. Comput Methods Appl Mech Eng 2006;196:595–607.